"Covalent Magnetism" and Invar-like Behavior within Ternary Nitrides: An *ab initio* Study

Samir F. Matar[a], Abdesalem Houari[b], Mohamed A. Belkhir[b], and Mirvat Zakhour[c]

[a] Institut de Chimie de la Matière Condensée de Bordeaux-CNRS, Université Bordeaux 1, Pessac, France
[b] Laboratoire de Physique Théorique, Département de Physique, Université de Bejaia, Route de Targua-Ouzemour, 06000 Bejaia, Algeria
[c] Laboratoire de Chimie Physique des Matériaux. Faculté des Sciences II, Université Libanaise-Fanar and Faculté des Sciences et de Génie Informatique, Université "Saint-Esprit" de Kaslik-Jounieh, Lebanon

Reprint requests to S. F. Matar. E-mail: s.matar@u-bordeaux1.fr

Z. Naturforsch. **2007**, *62b,* 881 – 890; received January 23, 2007

Dedicated to Dr. Bernard Chevalier on the occasion of his 60th birthday

Magnetic properties and bonding analyses of perovskite structure-derived TFe$_3$N (T = Ru, Os) nitrides have been investigated within density functional theory using both pseudo potential and all electron methods. At equilibrium, spin degenerate non-magnetic (NM) and ferromagnetic (FM) calculations of energy *versus* volume show that the ground state of the two compounds is ferromagnetic. Magnetic moments of Ru/Os and Fe, respectively, being situated at two different crystallographic sites are studied over a wide range of the cubic lattice parameter. The volume expansion indicates that iron atoms show itinerant magnetism while Ru and Os exhibit a localized behavior. Important magnetovolume effects are observed, with saturation of the magnetic moment reached in RuFe$_3$N but not in OsFe$_3$N. The electronic structure is visualized for the different binding characters Fe–N *versus* Ru/Os–N with the help of electron localization plots. The density of states of the ferromagnetic ground state is interpreted on the basis of a covalent magnetic model which goes beyond the Stoner rigid band model. An Invar-like behavior is predicted for the two nitrides.

Key words: Ternary Iron Nitrides, Magnetic Properties, Magnetovolume Effects, Invar-like Behavior, Covalent Magnetism

Introduction

Due to their potential applications, iron nitrides are of significant scientific interest. For example, in the field of high-density magnetic recording materials, Fe$_4$N was considered as a promising medium [1]. Since then several experimental and theoretical studies have been undertaken to elucidate its magnetic properties [2 – 5]. The cubic perovskite-derived structure of Fe$_4$N is shown in Fig. 1 (space group $Pm\bar{3}m$). With respect to the central nitrogen atom, two kinds of Fe atoms may be distinguished: Fe$^{\mathrm{I}}$ at (0, 0, 0) and Fe$^{\mathrm{II}}$ at ($1/2$, $1/2$, 0). As a consequence, Fe$^{\mathrm{I}}$ is likely to be less bonded to nitrogen and to be more 'labile' toward the effects of substitution with, *e. g.*, Os, Ir, and Ru. The effects of substitution of iron (at the corner sites) by other atoms (such as Ni, Pd, Ir, Os and Ru) on the magnetic properties of Fe$_4$N have been the subject of several studies [6 – 10]. Using Mössbauer spectroscopy, corner Fe (Fe$^{\mathrm{I}}$) was determined as the site of substitution within the structure [7] (see Fig. 1). In this latter study, the low amount of Os, Ir and Ru did not result in a significant change of the Fe$_4$N lattice parameter, and it was found that the substitution leads to the growth of very fine particles with superparamagnetic behavior. Eventually, at very high concentrations an ordered RuFe$_3$N and/or OsFe$_3$N antiperovskite structure should result. It is expected that the structural and magnetic properties of the substituted system will be different from those of pristine Fe$_4$N, and their study at a modeling level therefore has to be carried out in the proper framework of density functional theory DFT [11]. In this regard, not many reports treating Ru(Os)Fe$_3$N nitrides are found in the literature. In recent density functional-based calculations (using the FP-LAPW method) [12], a lattice pa-

0932–0776 / 07 / 0700–0881 $ 06.00

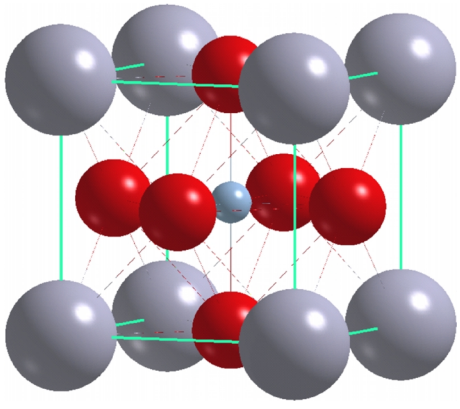

Fig. 1. (color online): The anti perovskite structure of Fe_4N, rewritten as $Fe^{I}Fe^{II}{}_3N$. Atom size from larger to smaller spheres follow the order: corner Fe^{I}, face center Fe^{II} and central N atoms. Ru and Os substitute for Fe^{I} in the ternary nitrides $RuFe_3N$ and $OsFe_3N$ studied here.

rameter very close to the experimental one for Fe_4N was calculated for $RuFe_3N$, which is stable in a ferromagnetic order. For the osmium system an *ad hoc* use of the Fe_4N lattice parameter in theoretical computations suggested a ferromagnetic ground state [13].

The present work follows our early and more recent theoretical [2, 26, 27] and experimental [7] investigations in proposing trends of the electronic and magnetic properties of the ternary systems TFe_3N (T = Ru, Os) with respect to pristine Fe_4N with an interpretation based on covalent magnetism on one hand and on potential Invar-like behavior from examining magneto-volume effects on the other hand. This property, which is known for the alloy system $Ni_{0.35}Fe_{0.65}$, whose compensation of the thermal α_T and the magnetic expansion α_M coefficients, which vary oppositely, leads to zero volume variation around r. t., was identified both experimentally and theoretically for the ternary nitride $NiFe_3N$ [10].

Computational Methods

As in our former works [2, 16, 26, 27], the self-consistent calculations were carried out in the framework of the well established density functional theory [11]. We mainly used the all electrons augmented spherical wave (ASW) method in a scalar relativistic implementation [14] due to the presence of heavy elements with $Z > 50$ such as Os. The exchange correlation effects were accounted for within the generalized gradient approximation (GGA) using the parameterization of Perdew, Burke and Ernzerhof [15]. This scheme was preferred over the LDA (local density approximation) in view of recent results on iron mononitrides [16]. In the ASW method, the wave function is expanded in atom-centered augmented spherical waves, which are Hankel functions and numerical solutions of Schrödinger's equation, respectively, outside and inside the so-called augmentation spheres. The transition metal *ns*, *np* and *(n–1)d*, n = 4, 5, 6 for Fe, Ru and Os, respectively, and N 2*s*, 2*p* states were used for the valence basis sets. For all calculations the ratio between the atomic radii of the corner Ru (Os), Fe and N atoms were kept constant: $r_{Ru(Os)}/r_{Fe}$ = 1.39 and r_{Fe}/r_N = 1.16. A sufficiently large number of k points was used to sample the irreducible wedge of the Brillouin zone, and the energy and charge differences between successive iterations were converged below $\Delta E = 10^{-8}$ Ryd. and $\Delta Q = 10^{-8}$, respectively, to obtain accurate values of the magnetic moments and accurate total energy differences between various ordered magnetic states. To extract more information about the nature of the interactions between the atomic constituents from electronic structure calculations, the crystal orbital overlap population (COOP) [17] or the crystal orbital Hamiltonian population (COHP) [18] may be employed. Both approaches provide a qualitative description of the bonding, nonbonding and antibonding interactions between two atoms. A slight refinement of the COHP was recently proposed in form of the "energy of covalent bond" (ECOV), which combines COHP and COOP to calculate quantities independent of the choice of the zero of potential [19]. Both COOP and ECOV give similar general trends, but COOP, when defined within plane-wave basis sets, exaggerates the magnitude of antibonding states. In the present work the ECOV was used for the chemical bonding analysis. In the plots, negative, positive and zero ECOV magnitudes are relevant to bonding, antibonding and nonbonding interactions, respectively.

In as far as no structural determinations are available for TFe_3N (T = Ru, Os), trends in cell volumes and ground state crystal structures were desirable in the first place. The equilibrium structures were obtained assuming spin degenerate systems from a full geometry relaxation of nitride systems starting from the Fe_4N structure and using a pseudo potential approach within the VASP code [20]. Ultra soft US Vanderbilt pseudo potentials (US-PP) [21] built within the GGA scheme [15] were used. The calculations were converged at an energy cut-off of 435.12 eV, sufficient for spin degenerate calculations, for the plane-wave ba-

sis set with respect to the k point integration with a mesh from $6 \times 6 \times 6$ to $12 \times 12 \times 12$ leading to 56 k irreducible k points. The tetrahedron method with Blöchl corrections [22] was applied leading from 141 to 1569 inequivalent tetrahedra. The Brillouin zone integrals were approximated using the special k point sampling of Monkhorst and Pack [23].

Geometry Optimization and Charge Distribution from Pseudo Potential Calculations

We started the geometry optimization of Fe_4N with an experimental lattice parameter of a = 7.1777 bohr (1 bohr = 0.529 Å). Then the lattice geometry was fully relaxed for the cell volume, shape and atomic positions. The same cell parameter was equally used for starting the calculations under the same conditions of convergence for both Ru and Os homologues. The resulting structures were all found cubic with an increasing lattice parameter along the series TFe_3N (T = Fe, Ru Os): $a(Fe_4N)$ = 6.966, $a(RuFe_3N)$ = 7.089, and $a(OsFe_3N)$ = 7.11 bohr. The smaller magnitude of $a(Fe_4N)$ with respect to the experiment of 2.95 % results can be expected in the framework of the approximations used. The obtained results are for a non-magnetic spin degenerate configuration; a full account of spin polarization effects will be done in the next section using the all electrons ASW method [14].

To get an insight in the real-space electronic structure of the nitride systems, an analysis of the electron localization function (ELF) introduced by Becke and Edgecomb [24] can be undertaken in the framework of US-PP calculations [20]. The ELF function is normalised between 0 (zero localization) and 1 (strong localization) with the value of $1/2$ corresponding to a free electron gas behaviour. By such a mapping one can illustrate the properties of chemical bonding. As an illustration for this class of systems ELF contour plots are shown for four cells of $OsFe_3N$ in Fig. 2. The planes chosen for a) and b) are, respectively, for $z = 0$, which comprises corner Os and face center Fe, and for $z = 1/2$ which comprises Fe and cell centered N atoms. Both plots point to a continuous electron distribution in between the atoms in a free electron-like localization (green color) contrary to both metal atoms which have no localization. This agrees with the chemical picture of a metal as made by a skeleton of ions surrounded by an electron gas. The nitride chemical picture, meaning negatively charged nitrogen, is stressed in Fig. 2b by the presence of a strong localization (red contours)

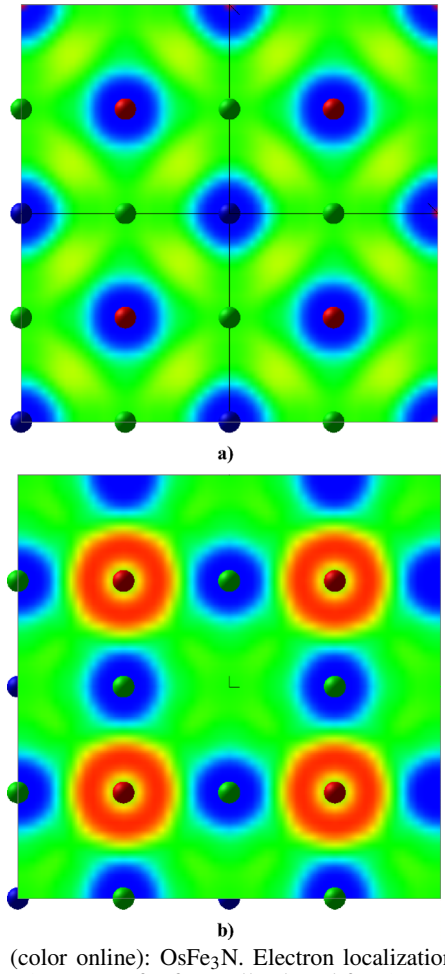

Fig. 2. (color online): $OsFe_3N$. Electron localization function (ELF) contours for four cells plotted for a) $z = 0$ plane comprising Os and Fe and b) $z = 1/2$ plane comprising Fe and N. Blue, green and red spheres are for corner Os, face center Fe and cell center N atoms, respectively (see Fig. 1). Blue, green and red ELF zones describe zero, free electron like and strong localization of electrons.

within the Fe_6N-like octahedron around N of which a projection can be seen. These illustrations stress furthermore the isolated character of the corner sites with respect to Fe_6N-like octahedra. In Fe_4N for instance the Fe^{I} moment is by $\sim 1\ \mu_B$ larger than that of Fe^{II}. This is explained on the basis of a larger localization of d orbitals at corner Fe sites. On the contrary, the Fe^{II} atoms which are covalently bonded to nitrogen, are consequently broadened and, due to spin pairing with N, carrying a lower magnetic moment. The replacement of Fe by isoelectronic Ru and Os, which are $4d$ and $5d$ elements with broad bands, should not sustain a magnetic moment. However, we shall see that

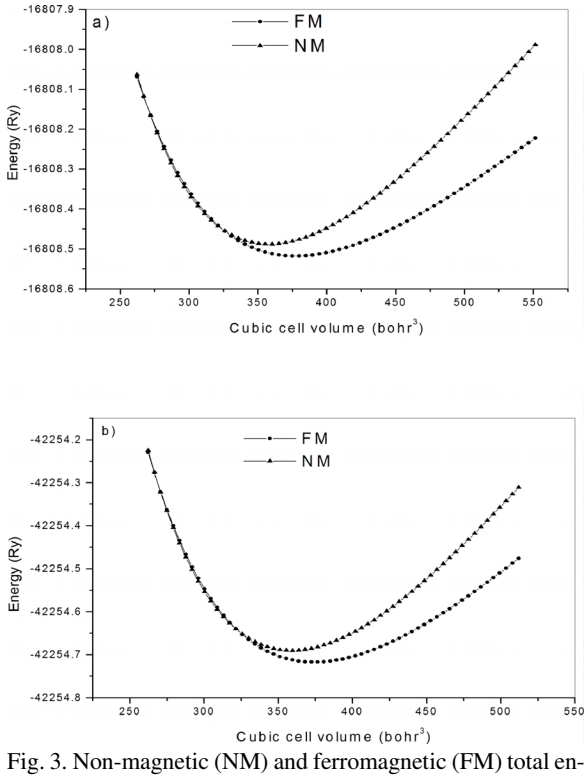

Fig. 3. Non-magnetic (NM) and ferromagnetic (FM) total energy *versus* volume curves for $RuFe_3N$ (a) and $OsFe_3N$ (b).

the localization of these *d* orbitals will allow an onset of atomic magnetic moments, which is an original feature of these elements, especially for osmium.

Electronic and Magnetic Structure Analysis with all Electrons ASW Method

Total energy and magnetic moments

The variations of the total energy *versus* volume of the unit cell for $RuFe_3N$ and $OsFe_3N$ were calculated over a wide range between 250 and 560 bohr^3, in both a non-magnetic (NM), *i. e.*, spin degenerate configuration, and then in a ferromagnetic (FM) one. The data allow us to determine the equilibrium volume (equilibrium lattice parameter), the bulk modulus and the corresponding stable magnetic order.

Fig. 3 shows the energy *versus* volume curves, which are fitted by a Birch-Murnaghan equation of state [25], for the two Ru(Os)Fe_3N nitrides. At the theoretical equilibrium volume, the ferromagnetic state is more stable than the non-magnetic one.

Table 1 summarizes the results of the total energy, the lattice parameter and the bulk modulus, obtained

Table 1. Calculated equilibrium properties (in atomic units (bohr): 1 Ry = 13.6 eV) for the nitrides $RuFe_3N$ and $OsFe_3N$ and of corresponding nitrogen free alloy systems, ES (empty spheres) replacing N. NM: non-magnetic and FM: ferromagnetic.

Equilibrium properties		E_0 (Ry)	a_0 (bohr)	B_0 (GPa)		m (μ_B)	H_{FC} (kG)
$RuFe_3N$	NM	−16808.48	7.094	292			
	FM	−16808.51	7.212	195	Ru	0.697	−470.68
					Fe	2.402	−150.63
					N	0.060	+4.06
					Tot	7.968	
$RuFe_3ES$	NM	−16698.72	7.094	–			
	FM	−16698.76	7.212	–	Ru	0.536	−973.80
					Fe	2.893	−336.35
					ES	0.043	−1.77
					Tot	9.261	
$OsFe_3N$	NM	−42254.68	7.103	302			
	FM	−42254.71	7.208	219	Os	0.392	−778.97
					Fe	2.192	−133.55
					N	0.050	+4.25
					Tot	7.022	
$OsFe_3ES$	NM	−42145.02	7.103	–			
	FM	−42145.02	7.208	–	Os	0.066	−4583.88
					Fe	2.467	−317.64
					ES	0.024	−1.63
					Tot	7.493	

at equilibrium volume. For $RuFe_3N$, a lattice parameter value of 7.094 bohr is obtained in the NM state, and of 7.212 bohr in the FM one. The former is close to the value obtained from geometry optimization (see above). For $OsFe_3N$, the NM and FM lattice parameters are 7.103 and 7.208 bohr, respectively. Again the agreement with the *ab initio* geometry optimization is good for the NM configuration at equilibrium. These values are larger than the Fe_4N lattice parameter (7.177 bohr) but should be smaller than the experimental one in view of the results, especially for Fe_4N. The fact that experimentally, no change was observed for $Fe_{(1-x)}Ru_xFe_3N$ [7] is certainly due to the low amounts of substitution $0.05 < x < 0.2$, and it appears that the results established recently in full-potential calculations [12] are somewhat underestimated. The bulk modulus B_0 is systematically larger for the NM state than for the SP configuration which follows from the larger lattice parameter of the latter and points to a larger compressibility when the system is magnetic. This means that the system is "softer" when it is magnetically ordered and "harder" when it is not.

Magnetovolume versus chemical effects

In a collective electron scheme, such as the one used here, the magnetization arises from interband spin po-

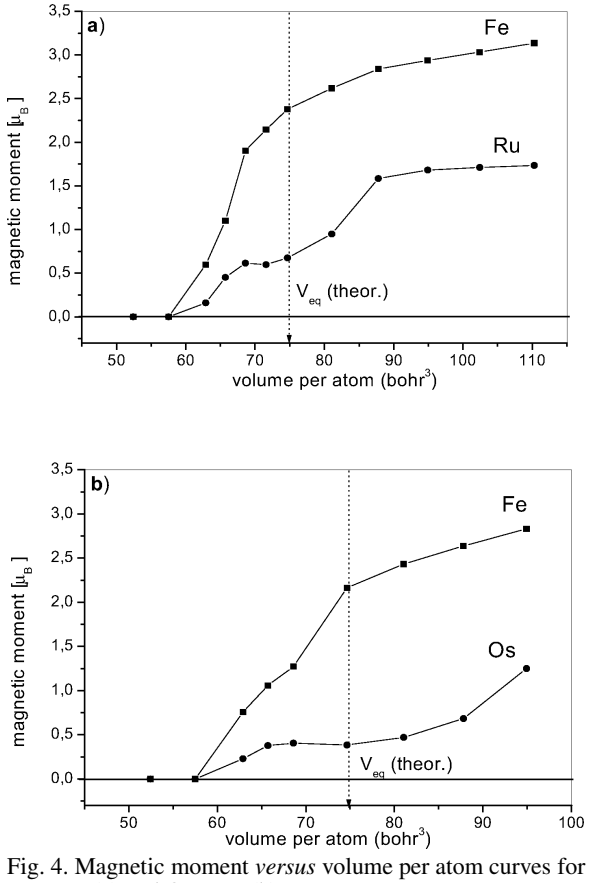

Fig. 4. Magnetic moment *versus* volume per atom curves for $RuFe_3N$ (a) and $OsFe_3N$ (b).

larization, *i. e.*, it is mediated by the electron gas. This is opposed to the localized electron moments where magnetization arises from intraband spin polarization such as in oxide systems, especially insulating ones. From this, it is expected that the magnetovolume effects will be large in intermetallic and insertion alloys systems such as those studied here as well as those formerly studied (Fe_4N and *fcc*-Fe) [26].

The variations of the magnetic moments with the cell volume for $RuFe_3N$ and $OsFe_3N$ are shown in Figs. 4a, b. At equilibrium, the magnetic moments of all atomic species, and thus those of the unit cell, are slightly larger in $RuFe_3N$ as compared to $OsFe_3N$ (see Table 1). For Ru a value of 0.697 μ_B (which agrees well with a previous report [12]) is obtained, whereas a somewhat larger value of 2.40 μ_B is obtained for iron in this compound. Smaller values are obtained in $OsFe_3N$ where Os and Fe possess 0.39 and 2.19 μ_B, respectively. The presence of relatively large moments on corner Ru and Os atoms results from the isolated character of these atoms with respect to the Fe_6N octahedron on the one hand and from the covalent mixing of their *d* states with those of face centered iron atoms at (1/2, 1/2, 0) through "covalent magnetism" on the other, which is developed in the next section. The larger Fe moments, with respect to Fe^{II} in Fe_4N [2], can be the consequence of the larger Fe–N distances and the Ru/Os–Fe metallic interaction. This is also further examined below.

From Fig. 4a, the Fe moment in $RuFe_3N$ increases rapidly with increasing volume to reach high values. At the large volume limit it does not reach saturation completely but its variation is small. The moment of Ru increases slowly towards a constant value around equilibrium; this is followed by an abrupt jump to higher values where it begins to saturate. The situation is similar in $OsFe_3N$ as shown in Fig. 4b. The Fe magnetic moment increases proportionally (almost linearly) with volume, whereas the Os moment remains constant over a wide range of volume around equilibrium (more pronounced than Ru) to finally increase at higher volume. Here, for both osmium and iron, saturation of the magnetic moment is not reached. From this kind of dependency, it is clear that an itinerant magnetism for iron has to be expected, while a more localized one is predicted for ruthenium and osmium as suggested above. The figures also show that for $RuFe_3N$ as well as for $OsFe_3N$ there is a clear collapse of the magnetic moment at some low volume (between a lattice parameter of 6.6 and 6.8 bohr) which can be reproduced under the conditions of high pressures. This transition is characteristic of an Invar-like behavior, which was reported for the other ternary iron nitrides $NiFe_3N$ and $PdFe_3N$ [10]. A property that points to the Invar behavior is the critical pressure P_c for the disappearance of magnetic order, $P_c = -2\Delta E/\Delta V$, where ΔE and ΔV are related to energy and volume differences between magnetic and nonmagnetic states, respectively. Computed values are $P_c(NiFe_3N) = 558$ kbar in agreement with experiment, *i. e.*, $P_c(\text{exp.}) = 530$ kbar from our early magnetostriction measurements [27]. This magnitude ranges between $P_c(Ni_{0.35}Fe_{0.65}) = 10$ kbar for the Invar alloy itself and $P_c \sim 4000$ kbar *fcc* γ-Ni. Hence, these two systems are labeled as "soft and hard" magnetic materials, respectively. From the values in Table 1 we derive the critical pressure criterion P_c. We find $P_c(RuFe_3N) = 487$ kbar and $P_c(OsFe_3N) = 547$ kbar, which are in the range of the $NiFe_3N$ values given above. These magnitudes allow the positioning of the two presently studied

systems within the range of $NiFe_3N$, identified previously as the first Invar-related nitride [10].

In order to establish the role played by nitrogen, complementary calculations were carried out with replacing the central nitrogen atom by an empty sphere (ES) within the atomic sphere approximation of the ASW method [14]. ES are pseudo atoms with zero atomic numbers and a valence basis set like nitrogen, so that they receive charges from neighboring atoms and allow for covalence effects within the structure. For this check we used the equilibrium lattice parameter obtained for NM and FM Ru(Os)Fe_3N. As can be seen in Table 1, total energies point again to a ferromagnetic ground state. The magnetization is larger than within the corresponding nitrides, and this is mainly due to an enhancement of the Fe moment while the moments on corner Ru and Os atoms are significantly lower. This could be due to a loss of covalency of the system without nitrogen. The role of nitrogen is hence not only to lower the moment on Fe due to the σ and π bonding within the Fe_6N-like octahedron, but to ensure a covalently bonded system. We can also note that the moments on N, which are relatively high in both nitrides, are not negligible on the ES, which is again a sign of covalency within the compounds. This is further detailed below in the discussion of the density of states and chemical bonding.

Hyperfine field, Fermi contact term

The effective magnetic field H_{eff} acting on the nucleus is usually written as the sum of four contributions

$$H_{\text{eff}} = H_{\text{i}} + H_{\text{FC}} + H_{\text{orb}} + H_{\text{dip}}$$

The internal field H_{i} is the magnetic field at the nucleus generated from the externally applied field. H_{FC} is the Fermi contact term of hyperfine interactions arising from unbalanced spin density of *ns* electrons at the nucleus (in non-relativistic description)

$$H_{\text{FC}} = -8\pi/3\,\gamma_{\text{N}}[\{\Phi\uparrow(0)\}^2 - \{\Phi\downarrow(0)^2\}]$$

where γ_{N} is the nuclear gyromagnetic ratio and the quantities between brackets are the densities of *ns* electrons at the nucleus (*i. e.*, $r = 0$) for $\uparrow$ and $\downarrow$ spin moments. This quantity is a major contribution to H_{eff}, and it can be obtained from calculations. H_{orb} and H_{dip} are the fields arising from the orbital magnetic moments (small for 3*d* elements) and from the dipole interactions with surrounding atoms. H_{dip} is zero for cubic symmetry as is the case in the systems under investigation.

In the case of $RuFe_3N$ we obtain $H_{\text{FC}} = -470.68$, -150.63 and $+4.06$ kG for Ru, Fe and N, respectively. A good agreement is found with the results of full-potential calculations [12] for this case. For $OsFe_3N$ our values differ from those of ref. [13] although they follow the same trend of magnitude. For instance, H_{FC}(Fe) = -133.55 kG comes close to the value of -122.5 kG in [13] where an *ad hoc* smaller lattice parameter than the one obtained by us was used for geometry optimization. As with respect to our early ^{57}Fe Mössbauer investigations of $Fe_{(1-x)}Os_xFe_3N$, $0 < x < 2$ [7], a hyperfine field magnitude of -212 kG on face centered Fe was found with a trend to decrease with increasing Os concentration. This could be due to the decrease of the transferred hyperfine field from largely magnetic corner Fe^{I} ($M \sim 3\ \mu_{\text{B}}$), $H_{\text{FC}} \sim -277$ kG to face centered Fe^{II} in Fe_4N when the amount of substitution is increased in the solid solution. Comparing the Ru and Os system one can note that the lowering of the H_{FC} value at Fe in the latter system is in agreement with the smaller magnetic moment.

Electronic band structure

In this section we discuss the electronic structure of $RuFe_3N$ and $OsFe_3N$ in line with that of the formerly studied Fe_4N [2] from the densities of states (DOS) and their weights as well as the chemical bonding properties using the ECOV criterion [19].

a) Density of states

Spin- ($\uparrow$ and $\downarrow$) and site-projected (Ru, Fe and N) partial DOS (PDOS), taking into account the multiplicity in the formula unit (1 Ru, 3 Fe, 1 N), are shown in Fig. 5a ($RuFe_3N$) and Fig. 5b ($OsFe_3N$). Those of Fe_4N (*i. e.*, $Fe^{\text{I}}Fe^{\text{II}}{}_3N$) are illustrated in Fig. 5c for comparison. Although included in the calculations as valence states, the N 2*s* states are omitted in Fig. 5. The energy shift between spin $\uparrow$ and $\downarrow$ population (due to the exchange splitting) is significant for Fe in both nitrides, which results in large magnetic moment values. In contrast, this shift is less important for Ru and Os, and consequently low values of their magnetic moment are obtained. The DOS of iron atoms are extended over a slightly larger energy window than those of Ru and Os. In the whole shape, these densities of states seem to be similar to those of Fe_4N, but with a careful analysis an important feature is noted. Contrary to Fe_4N (with

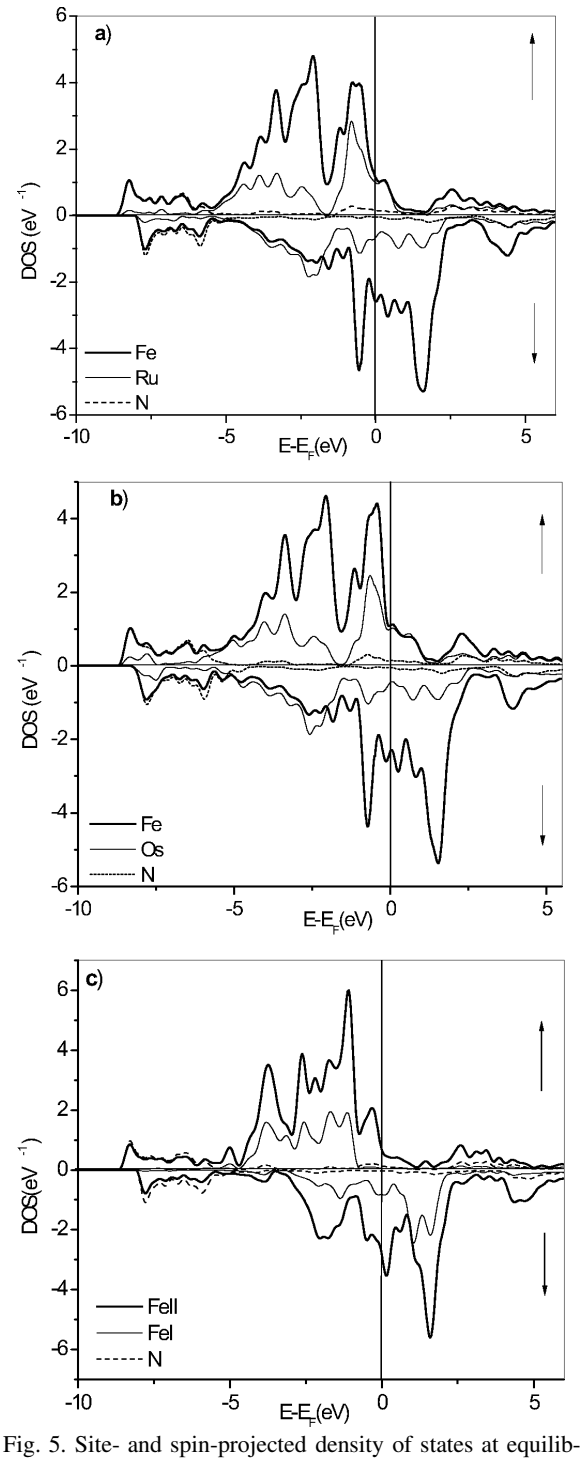

Fig. 5. Site- and spin-projected density of states at equilibrium. a) $RuFe_3N$, b) $OsFe_3N$, c) Fe_4N (partial DOS (PDOS) are drawn as: Ru, Os and Fe^I with thin lines, Fe/Fe^{II} with solid line and N with dashed line).

two iron substructures Fe^I and Fe^{II}) where Fe^I densities are low, somewhat large Ru and Os PDOS exist at energies around −6 eV, and this is more pronounced for Os. Although at this energy interval the N(2*p*)-Fe(3*d*) mixture is dominant (related to the stronger Fe–N chemical bond, which has a covalent character), the observed Ru and Os densities predict that significant Ru/Os–Fe and Ru/Os–N interactions exist. In Fe_4N, with the two Fe sites Fe^I and Fe^{II}, the Fe^I PDOS is very small at the Fermi level, hence the strong ferromagnetic behavior of Fe^I as opposed to the finite DOS value of Fe^{II} arising from Fe–N π^* bonding. On the contrary, Ru and Os densities exist at all energies up to the Fermi level. Although at this energy interval the N(2*p*)-Fe(3*d*) mixture is dominant (related to the stronger Fe–N chemical bond, which could be a covalent one), the observed Ru and Os densities predict that significant Ru/Os–Fe and Ru/Os–N interactions exist. As it was argued for $Ni(Pd)Fe_3N$ [10], it is proposed that the *p-d* hybridization of the Fe–N interaction increases the Fe *d* band width leading to states at the bottom and the top of the band. Furthermore, contrary to Fe_4N where the DOS of Fe^I drops to zero at E_F (Fig. 5c), indicating a strong ferromagnetic behavior, Figs. 5a, b show that the Fermi level E_F is still in the spin ↑ *d* band of Fe, Ru and Os. However, the major interaction is due to Fe–N π^* bonding. As a consequence, $Ru(Os)Fe_3N$ is a weak itinerant ferromagnet and responsible for the Invar-like behavior cited in the previous section. This feature agrees well with the variation of the magnetic moment *versus* volume.

b) Covalent magnetism

The weight difference between the spin ↑ and spin ↓ panels in the DOS figures (Fig. 5) is a feature which needs to be assessed. Generally, the magnetism of metals and alloys is correctly provided within the Stoner model [28] whereby the magnetic moment is the result of a rigid band shift of an initially non-magnetic (*i. e.*, with total spins) system to low-energy majority-spin (↑) DOS below the Fermi level (E_F) and to minority-spin (↓) DOS at higher energy (above E_F). However, early magnetic band calculations [29] allowed to identify a new feature exhibited by many intermetallic systems where the weights of the two spin populations DOS are not equal as proposed by the Stoner rigid band model. The result is a larger majority DOS weight with respect to the minority DOS on one hand and different partial DOS (PDOS) intensities in the spin down channel. This is also observed here (Figs. 5a and b).

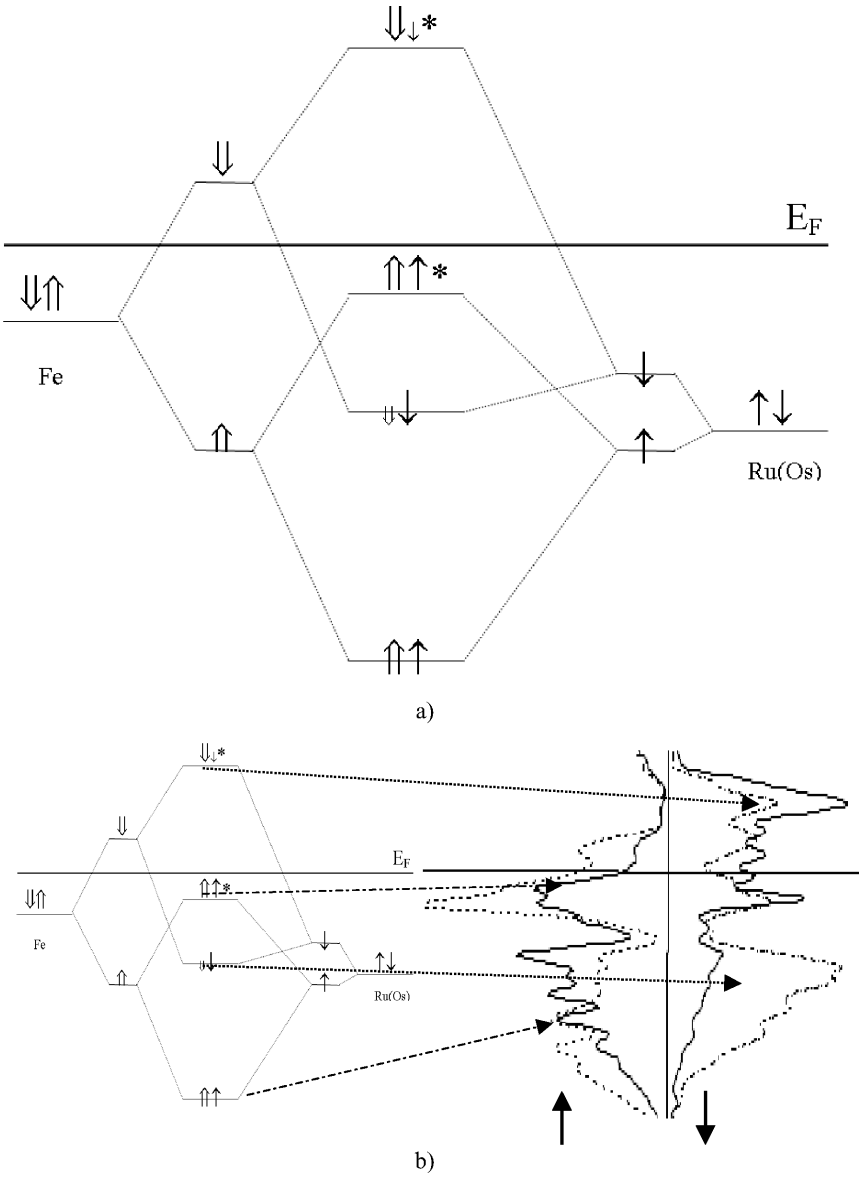

Fig. 6. Covalent magnetism. a) Simple molecular orbital sketch and b) correspondence between the MO-like diagram and the part of Figs. 5a, b corresponding to Ru(Os)–Fe DOS.

The model of "covalent magnetism" was therefore proposed to provide an explanation [28] going beyond the basic Stoner model.

Let us see how this concept performs for Ru(Os) Fe_3N using a representation familiar to chemists. In Fig. 6a, we provide a molecular orbital (MO) like diagram involving the two main metallic elements forming the nitride, namely Fe and Ru (Os). We also start from a spin-polarized configuration to draw the atomic-like orbitals (AO) which split in proportion to spin polarization to form the MO's. Fe will show larger splitting than Ru or Os due to the larger magnitude of its magnetic moment. Further, although Fe and Ru (Os) are isoelectronic, the respective Pauling electronegativities of 1.8 (Fe) *versus* 2.2 (Ru and Os) allow to position their orbitals at lower energy. For the sake of clarity we use double arrow symbols ($\Uparrow$ and $\Downarrow$) for Fe in order to point out clearly the differences with respect to Ru (Os) for which simple arrows $\uparrow$ and $\downarrow$ are used. Due to the filling of half of the *d* band with up to 5 electrons in both transition elements, the Fe $\Uparrow$ and Ru (Os) $\downarrow$ states are at the same relative energy. Now

we let the spin-split orbitals interact to form the MO diagram. States with like spins will be interacting. Fe and Ru (Os) spin (↑) levels will form a common majority spin band with bonding (⇑↑) and antibonding (⇑↑)* levels. For the spin ↓ states an energy difference occurs and the occupation with electrons will be in proportion with the starting AO levels. As a consequence, the Ru (Os) ↓ weight will be larger than ⇓ of Fe, *i. e.*, with more electron transfer from Ru (Os) to the MO for the minority spin MO bonding band, and *vice versa* for the antibonding band at higher energy, meaning that there is a larger electron transfer from Fe to the MO, and consequently that its PDOS weight will be larger. This is signaled by the relative magnitudes of the arrows. Now, if we illustrate the MO diagram with a PDOS picture, we obtain – almost – the same weight for majority spin for both Fe and Ru(Os) and a different picture of weights for the minority spin PDOS as shown in Fig. 6b which happens to be qualitatively reproduced by our MO scheme.

c) Chemical bonding properties

To illustrate the chemical bonding we examine the two-atom interactions from the spin-polarized ECOV [19] plots (covalence energy) assigning a bonding character (negative value) or anti-bonding character (positive value) to the interaction. This is shown for $RuFe_3N$ in Fig. 7. As one expects from exchange splitting, the majority spin ECOV are shifted to lower energies in both panels and one can see that the weights between ↑ and ↓ ECOV are not similar. For both spin populations the major part of the valence band is bonding; antibonding interactions start to appear around 1 eV below E_F mainly for the majority spin ECOV. The extension of the bonding metallic interaction for ↓ ECOV with larger magnitude than for Fe–N within the VB suggests that this bond favors the stabilization of the compounds. Note that this reproduces the qualitative MO scheme of Fig. 6 in assigning the antibonding Ru (Os)–Fe (⇑↑*) antibonding interactions just below E_F. The Ru–N interaction at the large $1/2\ a\sqrt{3}$ distance was found with small intensity. It is not shown here, but its presence certainly plays a role in the stabilization of the system and in the onset of magnetization on the corner atoms. The Fe–N interaction is bonding around −8 eV for both spin populations, reflecting a strong *d*-*p* hybridization of the Fe–N bond, but it starts to become antibonding below the Fermi level for spin ↑ ECOV. The same feature is observed in Fe_4N (Fe^{II}–N

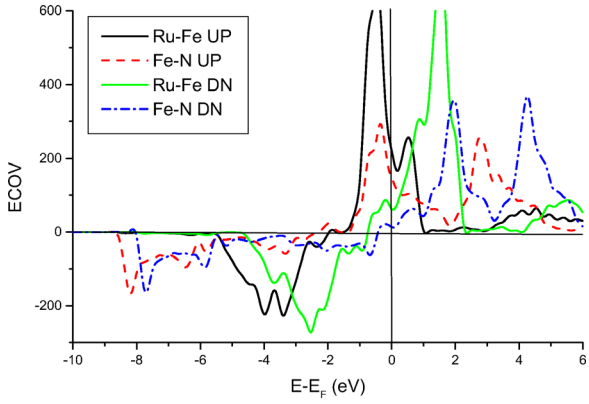

Fig. 7. (color online): Spin-resolved chemical bonding for Ru–Fe and Fe–N interactions from ECOV (negative and positive ECOC are for bonding and antibonding contributions, respectively).

interaction, see [30]). However, the major contribution to the stabilization of the polarized spin arises from spin down minority states for both major interactions within the structure.

Conclusion

In this study the electronic and magnetic structures of $RuFe_3N$ and $OsFe_3N$ with an ordered anti-perovskite structure were investigated. Full geometry optimization allowed to obtain equilibrium lattice parameters for the two systems using a pseudo potential DFT method. Then, using augmented spherical wave (ASW), all electron self-consistent calculations were carried out. From $E(V)$ curves the ferromagnetic state is preferred at equilibrium for the two compounds. A large exchange splitting is found for the Fe atoms, giving rise to a high magnetic moment, and non-negligible moments were identified for the corner Ru and Os as well as nitrogen atoms. The volume expansion makes the former to increase rapidly and to keep the latter almost constant at a high volume value. This implies that an itinerant magnetism of the Fe atom and a more localized one of Ru (Os) atoms are to be expected. The chemical role of nitrogen in lowering of the magnetization was also investigated by calculations on a nitrogen-free system. The density of states of different elements (Ru, Os and Fe) at the Fermi level makes the two nitrides globally weak ferromagnets. An important metallic interaction (Ru–Fe and Os–Fe) is expected, and by counteracting the Fe–N interaction it allows for larger magnetic moments at Fe (in face centered positions) as compared to its magnitude in Fe_4N.

The shape of the DOS is explained on the basis of the "covalent magnetism" approach through a sketch of an MO-type diagram which finds confirmation from PDOS and chemical bonding analyses. Finally, similar to what happens in related nitrides Ni(Pd)Fe_3N, the magnetic properties *versus* volume of Ru(Os)Fe_3N are strongly influenced by *p-d* hybridization of the Fe–N covalent bond. From the critical pressure of the vanishing magnetization, an Invar-like behavior is identified for the two nitrides.

Acknowledgement

We acknowledge computational facilities provided by the University Bordeaux 1 within the *M3PEC Mésocentre Régional* (http://www.m3pec.u-bordeaux1.fr) supercomputers partly financed by the "Conseil Régional d'Aquitaine" and the French Ministry of Research and Technology.

[1] D. Andriamandroso, G. Demazeau, M. Pouchard, P. Hagenmuller, *J. Solid State Chem*. **1984**, *54*, 34.
[2] S. Matar, P. Mohn, G. Demazeau, B. Siberchicot, *J. Phys. France* **1988**, *49*, 1761.
[3] S. Ishida, K. Kitawatase, *J. Magn. Magn. Mater*. **1994**, *130*, 353.
[4] A. Sakuma, *J. Magn. Magn. Mater*. **1991**, *102*, 127.
[5] R. Coehoorn, G. H. O. Daalderop, H. F. J. Jansen, *Phys. Rev. B* **1993**, *48*, 3830.
[6] R. S. De Fegueiredo, J. Foct, A. V. Dos Santos, C. A. Kuhnen, *J. Alloys. Compd*. **2001**, *315*, 42.
[7] D. Andriamandroso, S. Matar, G. Demazeau, L. Fournès, *IEEE Trans. Magn*. **1993**, *29*, 2.
[8] W. Zhou, L. J. Qu, Q. M. Zhang, D. S. Wang, *Phys. Rev. B* **1989**, *40*, 6393.
[9] G. Shirani, W. J. Takei, S. I. Ruby, *Phys. Rev*. **1962**, *126*, 49.
[10] P. Mohn, K. Schwartz, S. Matar, G. Demazeau, *Phys. Rev. B* **1992**, *45*, 4000.
[11] P. Honenberg, W. Kohn, *Phys. Rev*. **1964**, *136*, B864; W. Kohn, L. J. Sham, *Phys. Rev*. **1965**, *140*, A1133.
[12] C. Paduani, *J. Magn. Magn. Mater*. **2004**, *278*, 231.
[13] J. C. Krause, C. Paduani, *Physica B* **2005**, *367*, 282.
[14] A. R. Williams, J. Kübler, C. D. Gellat (Jr.), *Phys. Rev. B* **1979**, *19*, 6094; V. Eyert, *Int. J. Quantum Chem*. **2000**, *77*, 1007.
[15] J. P. Perdew, S. Burke, M. Ernzerhof, *Phys. Rev. Lett*. **1996**, *77*, 3865.
[16] A. Houari, S. F. Matar, M. A. Belkhir, *J. Magn. Magn. Mater*. **2007**, *312*, 298.
[17] R. Hoffmann, *Angew. Chem. Int. Ed. Engl*. **1987**, *26*, 846.
[18] R. Dronskowski, P. E. Blöchl, *J. Phys. Chem*. **1993**, *97*, 8617.
[19] G. Bester, M. Fähnle, *J. Phys.: Condens. Matter* **2001**, *13*, 11541 and 11551.
[20] G. Kresse, J. Hafner, *Phys. Rev. B* **1993**, *47*, 558; G. Kresse, J. Hafner, *Phys. Rev. B* **1994**, *49*, 14251; G. Kresse, J. Furthmüller, *Comput. Mat. Sci*. **1996**, *6*, 15; G. Kresse, J. Furthmüller, *Phys. Rev. B* **1996**, *54*, 11169.
[21] D. Vanderbilt, *Phys. Rev. B* **1990**, *41*, 7892.
[22] P. E. Blöchl, O. Jepsen, O. K. Anderson, *Phys. Rev. B* **1994**, *49*, 16223.
[23] H. J. Monkhorst, J. D. Pack, *Phys. Rev. B* **1976**, *13*, 5188.
[24] A. D. Becke, K. E. Edgecombe, *J. Chem. Phys*. **1990**, *92*, 5397.
[25] F. D. Murnaghan, *Proc. Natl. Acad. Sci. USA* **1944**, *30*, 244; G. Birch, *J. Geophys. Res*. **1978**, *83*,1257.
[26] P. Mohn, S. F. Matar, *J. Magn. Magn. Mater*. **1999**, *191*, 234.
[27] S. F. Matar, G. Demazeau, P. Hagenmuller, J. G. M. Armitage, P. C. Riedi, *Eur. J. Solid State Inorg. Chem*. **1989**, *26*, 517
[28] E. P. Wohlfarth, *J. Magn. Magn. Mater*. **1984**, *45*, 1.
[29] A. R. Williams, R. Zeller, V. L. Moruzzi, C. D. Gelatt (Jr.), J. Kübler, *J. Appl. Phys*. **1981**, *52*, 2067; for a recent review see: P. Mohn, *Magnetism in the Solid State. An Introduction*, Springer Series in Solid-State Sciences, Vol. 134, Springer, Heidelberg, **2003**.
[30] S. F. Matar, *J. Alloys. Compd*. **2002**, *345*, 72.